Finite Element Simulations of Ti6Al4V Titanium Alloy Machining to Assess Material Model Parameters of the Johnson-Cook Constitutive Equation

K. S. Vijay Sekar
vijaysekarks@ssn.edu.in
SSN College of Engineering
Department of Mechanical Engineering
603110 Chennai, TamilNadu, India

M. Pradeep Kumar
pradeep@annauniv.edu
Anna University Chennai
Department of Mechanical Engineering
600025 Chennai, TamilNadu, India

The machining of titanium alloys poses several inherent difficulties owing to their unique mechanical properties and cutting characteristics. Finite element (FE) simulations have reduced the burden of extensive experimental trials in understanding the deformation behavior and optimize the cutting process. The FE code relies on the qualitative nature of inputs such as material flow stress model, friction conditions, fracture criterions and the accuracy of the modeling process. The aim of this paper is to assess the performance of four material model sets of the Johnson-Cook (JC) constitutive equation in modeling the deformation behavior of Ti6Al4V alloy. The FE output at steady state conditions is compared with results from orthogonal cutting experiments on a tube of the work material. The effect of the parameters of the JC law and the capabilities of the constitutive equation are analyzed. The FE model is excellent in predicting the effective stress, strain and temperature, but produces marginal deviations in cutting force and chip morphology predictions and under predicts the feed forces. The material model constants computed through an evolutionary computational optimization process and those with conditions similar to machining produced good correlation with experiments.
Keywords: *titanium alloys, material constitutive models, orthogonal machining process, finite element simulation*

Introduction

Finite element simulations of machining processes are a boon to the manufacturing sector given its capabilities in optimization of tooling and production systems. The FE tools have significantly reduced the cost of design changes, improved the quality of the product and significantly reduced the lead time to manufacture. FE simulations have helped understand the machining behaviors of difficult to machine alloys like titanium (Obikawa and Usui, (1996), Baker et al., (2002), and Hua and Shivpuri, **(**2004)). Titanium alloys are an important class of aerospace materials with superior anti corrosion, anti oxidation and high strength to weight ratio. But the machining process is complex due to the unusual combination of high tensile strength and low thermal conductivity. FE simulations offer simple cost effective solutions to offset the cost of experimental trials. The success of a numerical model depends on the ability of the user to provide reliable and robust input data and conditions to the preprocessor of the FE code (Vaz Jr., 2000). Material property is one of the important inputs and this work focuses on the ability of the JC material law in providing accurate flow stress input to the code.

Umbrello (2008) studied the influence of three material model parameters of the JC model in modeling the conventional and high speed machining of titanium alloys concluding that flow stress parameters which were computed from conditions closer to machining (Lee and Lin, 1998) predicted the process variables better. Calamaz et al. (2008) proposed a new model for simulating titanium alloy machining and found good correlation with experimental data, better than the JC model. Shao et al. (2009) employed a thermodynamically constitutive equation to model the high speed machining process of Ti6Al4V and found reasonable prediction of temperature and tool wear depth with their model. The JC material constitutive law has been used by Umbrello (2008) effectively, while Calamaz et al. (2008) and Shao et al. (2009) developed their own models for simulations citing deficiencies in the JC law.

The JC law has been used extensively in numerical studies for deformation processes due to its flexibility in computing flow stress data suitable for FE codes. But there is a need to evaluate the applicability of different material model sets in the context of machining simulations. The JC material model parameter sets considered for this analysis are Lee and Lin (1998), Ozel and Karpat (2007), Khan et al. (2004) and Lesuer (2000).

The flow stress data from the four models is calculated for a range of strain, strain rate and temperature. This data along with thermo-physical properties of work and tool, friction conditions and fracture criterion are built into the FE model. The simulations are executed for cutting conditions identical to those employed in orthogonal machining of titanium alloy. A comparative study of the performance of the four different material model sets of the JC law is conducted. The JC material law was found effective in modeling the stress, strain and temperature, but produced marginal variations in cutting force and chip morphology predictions and under predicted feed forces. The material models suggested by Lee and Lin and Ozel and Karpat predicted the output better than others, since the parameters were computed from high strain applications and evolutionary computational process respectively.

Nomenclature

A = *yield strength, MPa*
B = *hardening modulus, MPa*
C = *strain rate sensitivity coefficient*
D = *material constant*
m = *thermal softening coefficient*
n = *hardening coefficient*
T = *temperature of the work material, K*
T_{melt} = *melting temperature of the work material, K*
T_{room} = *room temperature, K*

Greek Symbols

σ = *flow stress, MPa*
ε = *equivalent plastic strain*
ε' = *strain rate,* s^{-1}

Paper accepted November, 2010. Technical Editor: Anselmo E. Diniz

ε'_o = *reference plastic strain rate, s^{-1}*
ε_f = *effective strain*
σ_1 = *maximum principal stress, MPa*
τ = *shear stress, MPa*
μ = *coefficient of friction*
σ_n = *normal stress, MPa*

Johnson-Cook Material Model

The flow stress behavior of Ti6Al4V was modeled using Eq. (1), which was proposed by Johnson- Cook (1983) and describes the flow stress of the material as a function of strain, strain rate and temperature effects .The three terms represent the individual effects of strain hardening, strain rate hardening and thermal softening on the flow stress of the material undergoing deformation. The limitations of the JC model are inability to predict the flow stress at deformations below room temperature, lack of insight into interactions between strain, strain rate and temperature and lack of thermal softening phenomena (Calamaz et al., 2008). The JC model has been popularly employed to characterize the material deformation behavior of various materials due its suitability for use in FE codes.

$$\sigma = [A+B\varepsilon^{n}]\,[1+C\ln(\varepsilon'/\varepsilon'_o)]\,[1-\{(T-T_{room})/(T_{melt}-T_{room})\}^{m}] \quad (1)$$

where σ is the flow stress, ε is the equivalent plastic strain, ε' is the strain rate, ε'_o is the reference plastic strain rate, T is the temperature of the work material, T_{melt} is the melting temperature of the work material and T_{room} is the room temperature. Coefficient A is the yield strength, B is the hardening modulus, C is the strain rate sensitivity coefficient, n is the hardening coefficient and m is the thermal softening coefficient. The strain rate ε' is normalized with a reference strain rate ε'_o.

The JC models employed in this work are M1: Lee and Lin (1998), M2: Ozel and Karpat (2007), M3: Khan et al. (2004) and M4: Lesuer (2000). The M1 constants were identified from high strain rate mechanical testing using the Split Hopkinson Pressure bar (SHPB) method under a constant strain rate of 2000 s^{-1}, temperature range of 700-1100°C with a maximum plastic strain of 0.3. The M2 constants were computed using an evolutionary computational algorithm called cooperative particle swarm optimization (CPSO). It uses a fine grained search method integrated into Matlab programs which when linked with flow stress determination computer program help identify the optimized JC constants. The M3 constants were optimized through a combination of SHPB and the least square technique. The M4 constants were computed through least square techniques fitted to a power law equation. The various model parameters were chosen based on the nature of experiments and procedures used to compute the flow stress data. Only the Lee and Lin model has been employed for such a purpose (Umbrello, 2008) prior to this work. Table 1 shows the JC model material constants employed in this work.

Table 1. JC material constants for Ti6Al4V.

JC Models	A(MPa)	B(MPa)	C	n	m
M1: Lee and Lin (1998)	782.7	498.4	0.028	0.28	1
M2: Ozel, Karpat (2007)	987.8	761.5	0.01516	0.41433	1.516
M3: Khan et al. (2004)	1104	1036	0.01390	0.6349	0.7794
M4: Lesuer (2000)	1098	1092	0.014	0.93	1.1

Orthogonal Cutting Experiments

The orthogonal cutting experiments were performed with a tube of Ti6Al4V alloy on a Lathe Machine tool under dry conditions. The cutting speeds used were 25, 40, 61 and 93 m/min with a constant feed rate of 0.191 mm/rev. An advanced cutting tool with a pressure vapor deposition of titanium aluminum nitride coating on tungsten carbide-cobalt base material was used. The cutting speed was varied while the feed rate was kept constant for each cutting cycle. The depth of cut was equal to the tube thickness of 2 mm. The cutting forces were recorded through a Kistler dynamometer (Type 9257 B) attached to the tool post which was connected to the data acquisition software through a charge amplifier. The chips collected were observed under a high resolution scanning electron microscope (SEM) which captures and plots the calibrated chip morphology. The chips were cleaned and mounted on a circular fixture and rotated to view the image across the chip thickness. A natural image of the titanium chip is captured to visually present the structural deformation caused by the machining process. The measurements for the segmented chips were read across the length of the chip and the average values for peak, pitch and valley tabulated. The chip thickness was measured with a digital micrometer and the chip thickness ratio (CTR – ratio of depth of cut and chip thickness) calculated. Table 2 shows the experimental set up for machining Ti6Al4V alloy.

Table 2. Experimental set up for machining Ti6Al4V alloy.

Work material	Ti6Al4V alloy (Tube)
Work dimensions (mm x mm)	320 x 59.3 (length x outer diameter)
Tube thickness (mm)	2
Tool material	PVD coated tungsten carbide insert
Tool rake angle	−5°
Tool clearance angle	+5°
Tool make	CNMG 120408 MP , KC 5010, Kenna metal
Cutting Speeds (m/min)	25, 40, 61 and 93
Feed rate (mm/rev)	0.191
Cutting conditions	Dry
Dynamometer	Kistler, Type 9257 B

Finite Element Modeling and Simulation

FE model

The finite element modeling was performed in Deform-2D™ which is based on an updated Lagrangian formulation which considers the mesh to be attached to the work piece during deformation. The chip shape develops as a function of the deformation process, process parameters and material properties and hence need not be predetermined. The work material was fully constrained while the tool material was allowed movement in the x axis. The thermo-physical properties of the work and tool materials and the flow stress data of Ti6Al4V alloy calculated from the material models were incorporated into the FE model. The work piece was modeled as plastic and the tool as rigid materials. A 7 x 2 rectangular cross section was considered for the work piece geometry and meshed with 5900 four noded iso parametric quadrilateral elements with an elemental width of 0.04775 mm and an aspect ratio of 1 to ensure a high density mesh. The tool geometry incorporating the rake and clearance angles of the tool used in the experiments was meshed with 250 elements. The

simulation was carried out with a plane strain assumption and the cutting conditions were identical to the experiments. An automatic re meshing algorithm integrated in the FE code ensures the continuity of the chip formation process. The simulated results are viewed through the post processor and the results are noted at near steady state conditions. An iterative convergence procedure based on trial and error was employed to improve the predictions for cutting force and chip morphology. The FE model and chip formation are shown in Figs. 1(a) and 1(b).

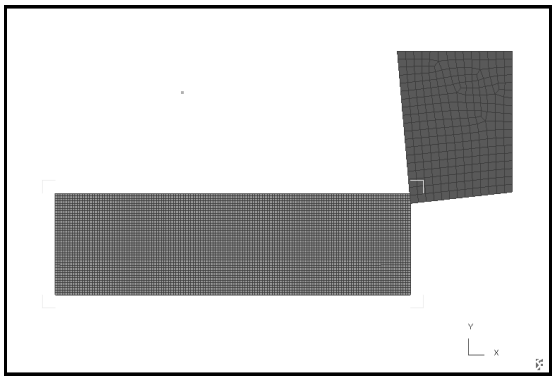

Figure 1(a). FE model.

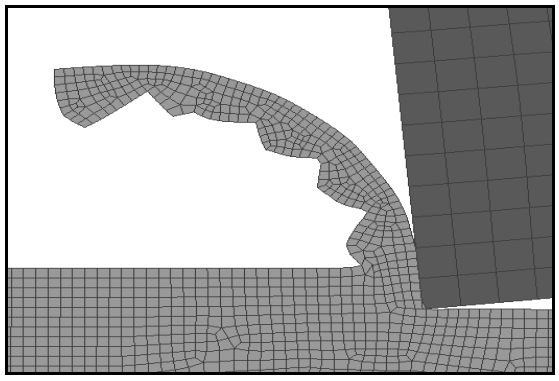

Figure 1(b). Chip formation model.

Fracture criterion

The Cockroft and Latham (1968) criterion given in Eq. (2) was employed in the FE code to account for the fracture phenomena which cause segmented chips typical of titanium alloys even at low cutting speeds. It states that fracture occurs when the integral of the largest tensile principal stress component over the plastic strain path reaches the critical damage value, *D*.

$$\int_0^{\varepsilon_f} \sigma_1 d\varepsilon = D \tag{2}$$

where ε_f is the effective strain, σ_1 is the maximum principal stress and *D* is a material constant. The critical damage value is computed for every element at each time step and initiates a crack when this value is reached in two steps: (i) the element is deleted with all parameters related to it and (ii) the rough boundary produced by element deletion is smoothed by cutting out the considered rough angle and adding new points.

Friction modeling

The constant coulomb friction model given in Eq. (3) was employed in the FE code to model the friction characteristics of Ti6Al4V alloy machining. The simple friction law was chosen since it has been proved that coefficient of friction is more relevant to frictional modeling than the law on which it is based and the forces data are sufficiently reliable and less sensitive over a wide range of frictional values from 0.2 to 0.8. (Filice et al., 2007).

$$\tau = \mu\sigma_n \tag{3}$$

where τ is the shear stress, μ is the coefficient of friction and σ_n is the normal stress. The shear stress is expressed as a product of Coulomb friction coefficient with the normal stress.

The FE simulation is performed with available μ and *D* values [Deform User manual] and the cutting force and chip morphology compared with experiments. The μ and *D* values are modified till there is no appreciable change in the cutting forces and chip morphology outputs measured. In this work a μ value of 0.3 and *D* value of 100 was employed for the comparative study.

Results and Discussion

The FE results for cutting force, feed force, chip morphology, effective stress, strain and temperature with the four input material model sets are presented here. The analysis is presented for a cutting speed of 93 m/min and feed of 0.191 mm/rev except for cutting force and feed force where all the speeds are discussed. The cutting speed and feed represent the highest cutting conditions in this study. The FE output was measured at near steady state conditions to ensure better comparison with experiments.

Cutting force

Figure 2 depicts the cutting force predictions of the FE models against the experimental results. The experimental cutting force decreased with the cutting speed from 25 to 40 m/min and showed a marginal increase between 40 to 61 m/min and gradually declined from 61 to 93 m/min. The marginal increase is due to the strain hardening effect which alters the trend slightly and then the decrease between 61 and 93 m/min is due to the increased cutting temperature which results in thermal softening of the work material. The cutting forces and therefore the cutting power required to machine the material thus increase with strain hardening of the titanium alloy and decrease with increasing cutting temperature.

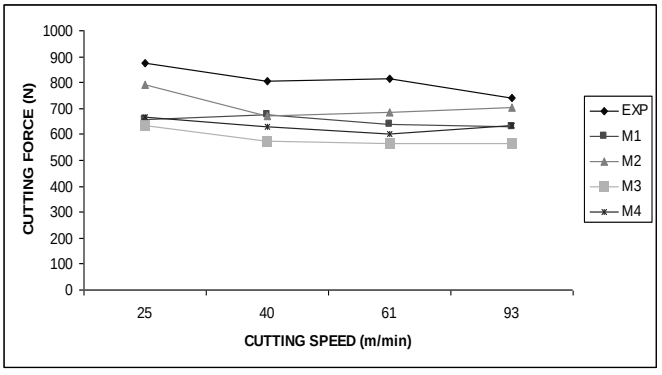

Figure 2. Comparison of experimental and FE cutting forces.

The FE predictions with M2 model at cutting speeds of 25 m/min (−9.38%), 61 m/min (−15.86%) and 93 m/min (−5.39 %) and the predictions with M1 model at 40 m/min (−16.35%) produced the closest correlation with average experimental cutting forces (value in brackets indicate the error percentage in comparison to experiments). The M2 model results especially at 93 m/min can be attributed to the optimized material constants obtained through a fine grain search algorithm and advanced cooperative particle swarm optimization technique. The parameter *A* which represents the initial yield strength of titanium alloy appears a fine tuned one and has impacted the cutting force results. The M1 model whose parameters were obtained by SHPB through high strain rate mechanical tests yielded the next best results since the experimental conditions were closer to actual machining. Model M4 predictions were moderately comparable to M1, M2, but certainly better than model M3. The reason for the M4 results can be attributed to the computation of flow stress data at strain rates around $10^4 s^{-1}$, while the poor prediction of the model M3 could be due to the low range of strain rates (10^{-5}, 10^{-3}, 1 and 3378 s^{-1}) and temperature (755 K) employed in the uni-axial loading tests performed to compute the flow stress.

Feed force

Figure 3 shows the graphical comparison of experimental and simulated feed forces for various cutting speeds. In general, the experimental feed forces were around two thirds of the cutting forces and the same trend is followed in the predictions too. The feed force predictions were less accurate than the cutting force predictions across all cutting speeds. The experimental feed force initially decreased till a cutting speed of 40 m/min and then gradually increased till 93 m/min. All the four material models showed a gradually decreasing trend throughout with a marginal increase shown by models M3 and M4 at 93 m/min.

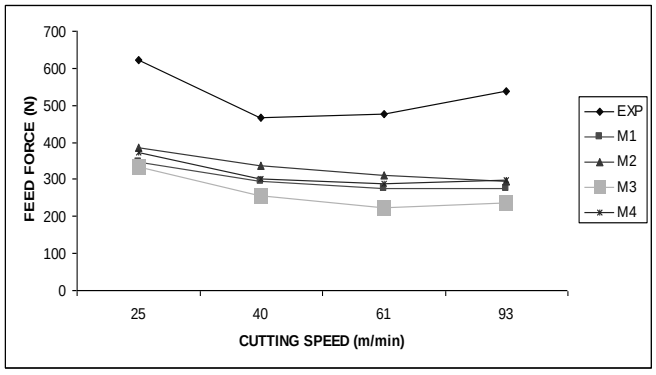

Figure 3. Comparison of experimental and FE feed forces.

Model M2 with optimized flow stress parameters predicts better than other models at 25 m/min (−37.84%), 40 m/min (−28.20%) and 61 m/min (−34.66 %), while model M4 (−44.89%) at 93 m/min was marginally better than M2. The predictions of model M1 was comparable to M2 and M4 while M3 predictions were below par. The variations suggest that the feed force is affected by the five parameters of the JC law. The under prediction of feed forces raises an important question regarding the direct application of existing constitutive laws for characterizing feed forces in titanium alloy machining.

Feed forces are impacted by friction coefficient and friction law as well, generally the higher the friction value, the higher the feed force predictions. In this work, a coulomb friction of $\mu = 0.3$ was employed for all the four models to ensure uniformity in friction modeling. The coulomb friction law ensures that frictional stress on the rake face of the tool is calculated from the normal stress acting on the same surface and not from the shear yield stress of the material, which results in large frictional forces. Hence, the coulomb law of friction yields higher feed forces than a shear frictional law. A μ value higher than 0.3 increases the feed force predictions but significantly affects the chip formation process and results in over estimation of cutting forces. A balance needs to be achieved between use of higher friction coefficients and the need to ensure a steady state chip formation process. However, optimization of the material flow stress parameters might result in an appropriate flow curve, which could improve the feed force predictions. The discrepancy in feed force predictions have been reported by Halil et al. (2004) when using three different FE codes and more recently by Calamaz et al. (2008) in significant works. It can be concluded that feed forces are sensitive to frictional coefficient and frictional law and the JC material flow parameters. Fine tuning these parameters might improve feed force predictions. The effect of tool-tip radius (value used in modeling same as the experimental one) and chip separation criterion (based on the critical damage value of the Cockroft-Latham law which is inbuilt in Deform 2D) in feed force predictions are not apparent since the predictions for cutting forces and chip geometry are reasonably good with the values employed in this work. However, detailed studies related to the above phenomena need to be carried out to investigate the case. In the present circumstances, model M2 seems capable of better feed force predictions than other models.

Chip morphology

Figures 4(a) and 4(b) show the actual and SEM photograph for chip morphology respectively. The average peak, valley, pitch and CTR (ratio of uncut chip thickness to chip thickness) were measured from the SEM image and compared with experimental chips measured with a digital micrometer. Figures 5(a), 5(b), 5(c), 5(d) and 5(e) show the comparison between experimental and predicted chip shapes.

4(a). Actual Photograph.

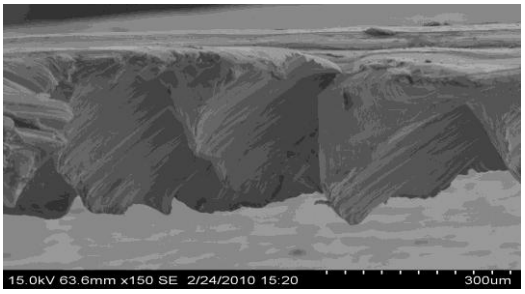

4(b). SEM photograph.

Figure 4. Experimental chips.

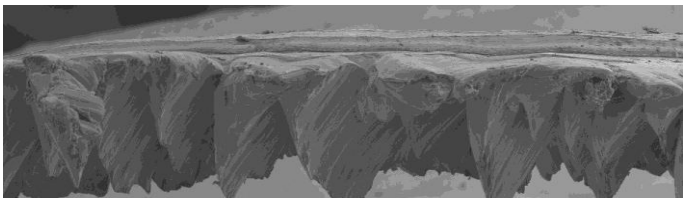

5(a). SEM photograph of Experimental chip shape.

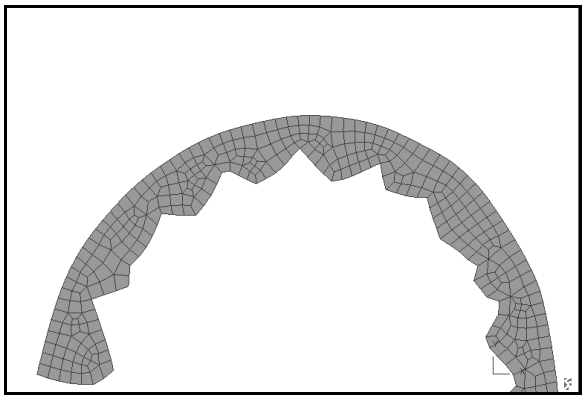

5(b). M1.

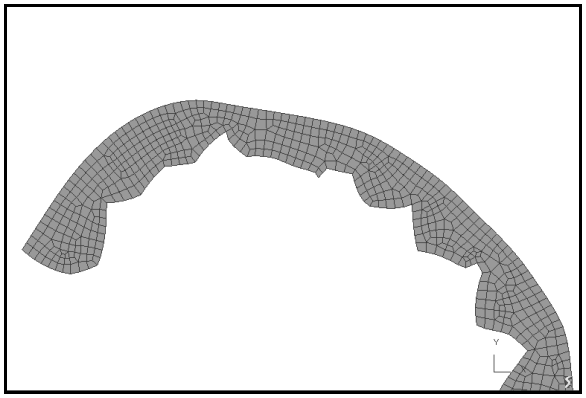

5(c). M2.

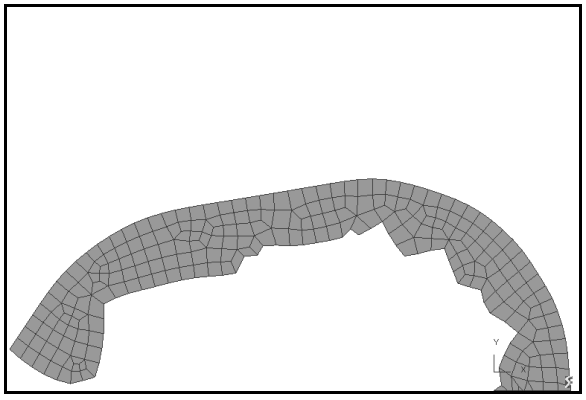

5(d). M3.

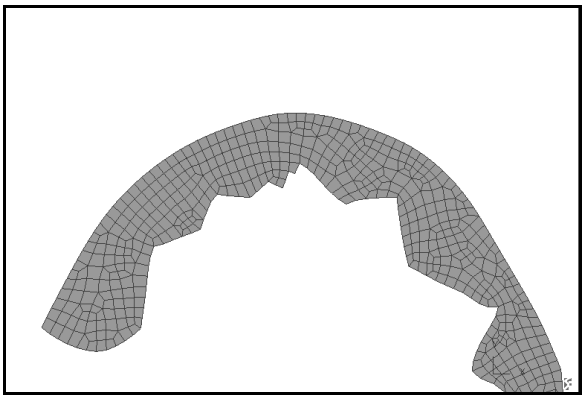

5(e). M4.

Figure 5. Experimental and Predicted chip shapes for the FE models.

The FE predictions with models M2 and M3 simulated chip curls with lesser radius similar to experiments, while M1 and M4 predicted large curl radius. The average pitch, peak, valley and CTR for the simulated chips were measured through dimensions of the deformed element coordinates. Model M1 predictions for pitch and valley, M2 for peak and M1, M2 for CTR compared well with experiments. All the models over predicted the average valley parameter. Model M1 predictions for most variables were better than other models. In general, all the models predicted irregular chip shapes, which could be attributed to the instability that arises due to interactive competition between strain hardening and thermal softening phenomenon that produces irregular oscillations at low speeds and usually disappears at high speeds leading to asymptotic periodic oscillations (Davies and Burns, 2001). Table 3 shows the error estimations in chip morphology with the FE models.

Table 3. Error estimation for the simulated chip geometry of the FE models.

	Chip morphology (µm)			CTR
	Pitch	**Peak**	**Valley**	
Experimental value	210	291	67	0.66
M1	303	267	165	0.71
(Error %)	(+44.28)	(−8.24)	(+146.26)	(+7.57)
M2	326	313	189	0.61
(Error %)	(+55.23)	(+7.56)	(+182.08)	(−7.57)
M3	304	265	169	0.72
(Error %)	(+44.76)	(−8.93)	(+152.23)	(+ 9.09)
M4	369	314	191	0.60
(Error %)	(+75.71)	(+7.90)	(+185.07)	(−9.09)

Stress distribution

Figure 6 shows the predicted effective stress distribution with the FE models. The von mises stress plot for all the four cases reveal maximum stresses at the primary deformation zone where the tool is in contact with the work material. The negative rake angle causes greater stress on the work and the tool at the point of contact. The stress on the machined surface is residual in nature while the stress values decrease around the uncut surface and the deformed chip. The four models show good consistency in modeling these

phenomena, suggesting that the JC law is good when addressing a global output like stress.

The models M1 and M2 predict similar ranges (180-1620 MPa) for effective stress suggesting that the material constants of the two models combine to produce similar stress patterns during machining. Models M3 and M4 predicted marginally lower ranges.

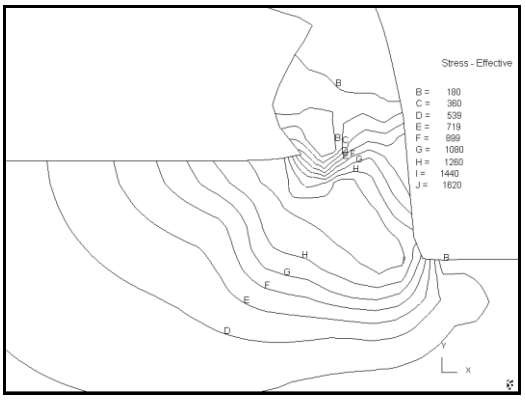

6(a). M1.

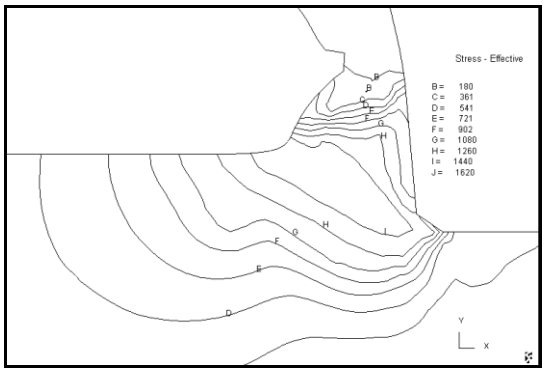

6(b). M2.

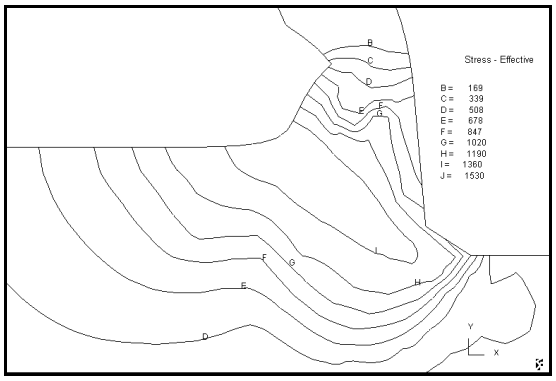

6(c). M3.

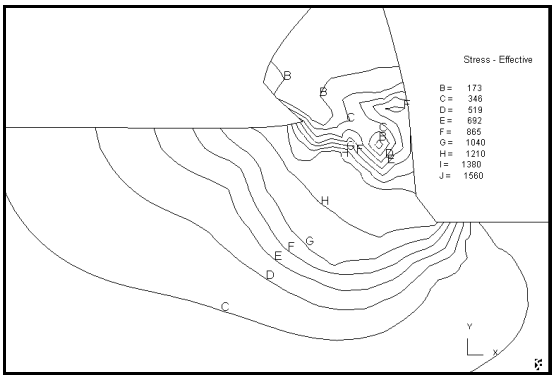

6(d). M4.

Figure 6. Effective stress distributions for the FE models.

Models M2 and M3 show uniform stress distribution across the three deformation zones while M1 and M4 show stress concentration near the formation of segments. Model M4 also shows uneven stress distribution at the secondary and primary deformation zones respectively.

Strain distribution

Figure 7 shows the experimental and predicted effective strain distribution for the FE models. The plastic strain is higher at the primary shear zone followed by the secondary shear zone and least at the free end of the chip. The SEM chip shows regions of high and low strain across the chip thickness, suggesting a complex chip formation mode which results in serrations and segments even at low cutting speeds. In other materials this phenomenon is present only in high cutting speed machining. The simulated chip for the four models present similar strain patterns. The strain filed in the free end of the chip is identical for all the models. There appears to be minor variations in the primary and secondary deformation zones.

The higher stress near the shear plane for models M1 and M2 should suggest higher deformations, but only model M2 replicates this proposition. Models M4 and M3 show higher deformations at the shear plane and tool chip contact respectively. It can be concluded that Model M2 with an optimized strain hardening exponent '*n*' is a good tool for predicting plastic strain path of titanium alloy. A strain softening phenomena to account for stress increase at reduced strain has been employed by Calamaz et al. (2008) to good effect in their new material model.

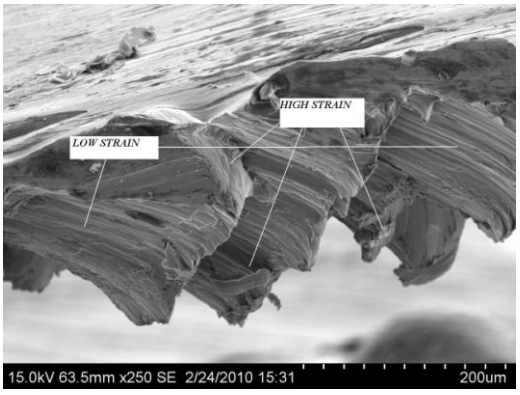

7(a). SEM chip strain distribution.

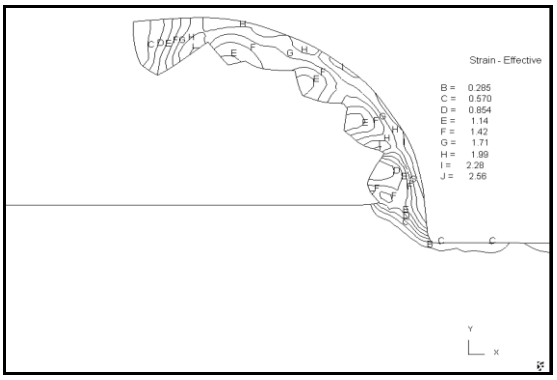

7(b). M1.

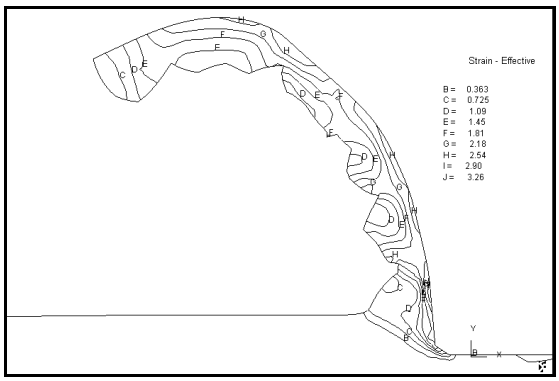

7(c). M2.

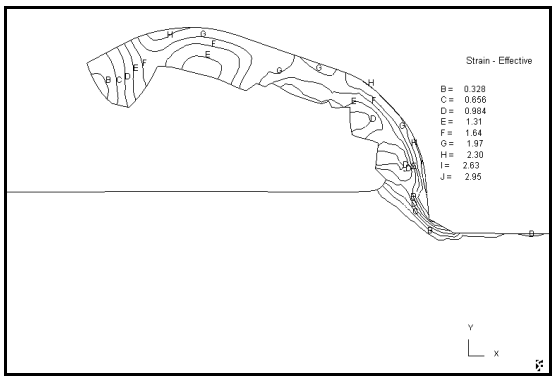

7(d). M3.

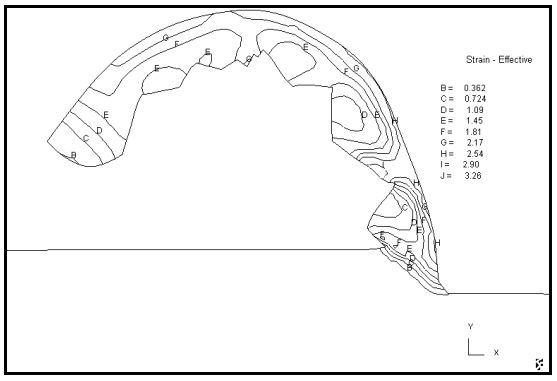

7(e). M4.

Figure 7. Effective strain distributions for experimental chip and FE models.

Temperature distribution

Figure 8 shows the temperature distribution for the various FE models. Heat transfer in the machining process takes place primarily in the shear zone where the plastic work is converted into heat and the chip-tool interface where frictional heat is generated. Some heat is lost to the ambience through convection and some transferred to the outgoing chip and the cutting tool through conduction. The low thermal conductivity of titanium alloys ensures poor heat dissipation, resulting in rapid wear of the cutting tool and reduction in tool life. Hence cutting fluids and cryogenic coolants are necessary to quickly remove the latent heat. In the FE model the work material is treated as plastic and the tool as rigid to facilitate better understanding of the heat transfer due to plastic deformation of titanium alloy during machining. Hence, the thermal analysis is concentrated on the work material alone. The temperatures reach steady state quickly after the initial increase in the primary and secondary deformation zones. The experimental temperature is usually the highest at the chip-tool interface (secondary deformation zone) followed by the shear plane (primary deformation zone) and least in the uncut surface. The simulated maximum temperatures are more within the chip due to the low thermal conductivity which does not allow quick heat dissipation from the deformed chip. The temperature distribution in the primary and tertiary zones is as expected in the machining process.

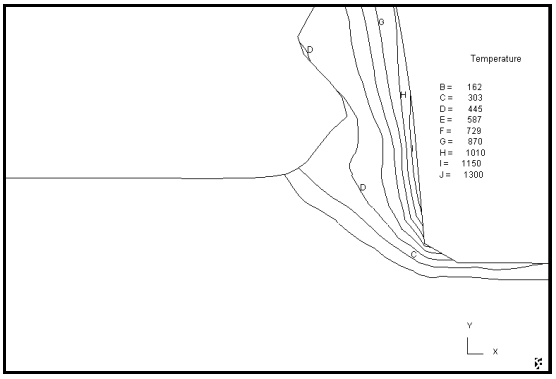

8(a). M1.

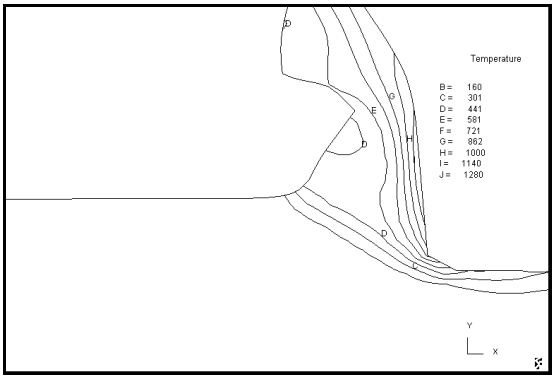

8(b). M2.

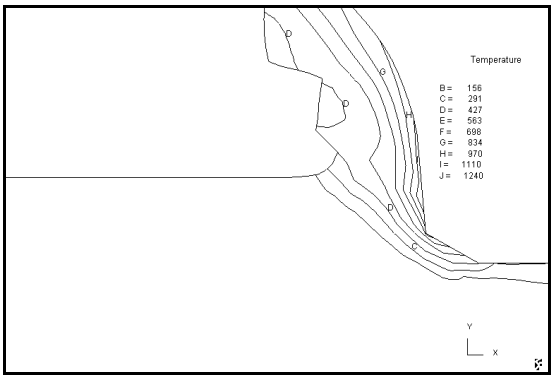

8(c). M3.

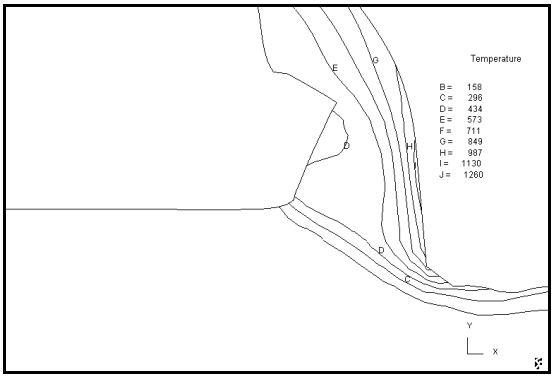

8(d). M4.

Figure 8. Temperature distributions for the four FE models.

The four material models show good agreement with each other in predicting the temperature pattern in titanium alloy machining. The marginal variation in temperature maxima for the four models could be attributed to the variation in the value of '*m*', the thermal softening coefficient in the four models. The effect of cutting speed and friction modeling also has an effect on the temperature distribution. Generally, the FE predictions for temperature are likely to show lesser than normal values (as observed in literature), because of the short cutting process simulation which prevents the temperature from reaching steady state. The predictions of model M1 with flow stress computed from high strain rate mechanical testing and at high temperatures appear marginally better than other models.

The good correlation of the four material model parameters suggests that the JC law is suitable for thermal modeling of titanium alloy machining.

Conclusions

The aim of the present work is to investigate the effect of four sets of material model parameters of the JC model in predicting the cutting force, feed force, chip morphology, stress, strain and temperature of the orthogonal machining process of Ti6Al4V titanium alloy. The flow stress data from the four different material model parameters were input to the FE code and a FE model was built to replicate the orthogonal cutting process. The cutting force, feed force and chip morphology were evaluated against the experimental results and the effective stress, strain and temperature analyzed for all the models. The following conclusions are made.

Model M2 developed by Ozel and Karpat (2007) predicted the cutting forces with good correlation to the experiments indicating its superior material constants found by evolutionary computational algorithms. The optimized values of the five constants obtained through a fine grain search process increase the capability of the model in phenomenological representation of the cutting characteristics of Ti6Al4V alloy. Model M1 developed by Lee and Lin (1998) employing conditions from SHPB through high strain rate mechanical testing predicted the chip morphology better than other models. All the models under predicted the feed forces with predictions of M2 marginally better than others. The poor prediction could be attributed to the friction model and the sensitivity of the JC parameters. Model M2 predictions for effective stress and strain and model M1 predictions for temperature were marginally better than other FE models. The good predictions of M1 and M2 can be attributed to the computation of material parameters which produce flow stress data matching practical machining tests.

All the four models predicted the global phenomena of stress, strain and temperature with good correlation to each other. This proves the robust nature of the JC constitutive equation in aptly modeling the deformation behavior from a global view point. It is necessary to develop constitutive models based on machining tests and also explore methods to optimize and fine tune the individual parameters for application to numerical simulations.

The FE model and the assumptions of friction and fracture criteria in this work are found suitable to model the machining characteristics of titanium alloy and assesses the relative merits and demerits of the employed flow stress model parameters.

Acknowledgement

The Authors wish to acknowledge the contribution of the Central workshop of the Mechanical Department at the College of Engineering, Guindy, Anna University, Chennai, India, for providing the infrastructure for the experimental work.

References

Baker, M., Rosler, J. and Siemers, C., 2002, "Finite element simulation of segmented chip formation of Ti6Al4V", *Journal of Manufacturing Science and Engineering*, Vol. 124, pp. 485-488.

Calamaz, M., Coupard, D. and Girot, F., 2008, "A new material model for 2D numerical simulation of serrated chip formation when machining titanium alloy Ti-6Al-4V", *International Journal of Machine Tools and Manufacture*, Vol. 48, pp. 275-288.

Cockroft, M.G. and Latham, D.J., 1968, "Ductility and workability of metals", *Journal of Institute of Metals*, Vol. 96, pp. 33-39.

Davies, M.A. and Burns, T.J., 2001, "Thermomechanical oscillations in material flow during high- speed machining", *Philosophical transactions of the Royal society of London A*, Vol. 359, pp. 821-846.

Filice, L., Micari, F., Rizzuti, S. and Umbrello, D., 2007, "A critical analysis on the friction modeling in orthogonal machining", *International Journal of Machine Tools & Manufacture*, Vol. 47, pp. 709-714.

Halil Bil., Engin Kılıc, S. and Erman Tekkaya, A., 2004, "A comparison of orthogonal cutting data from experiments with three different finite element models", *International Journal of Machine Tools & Manufacture*, Vol. 44, pp. 933-944.

Hua, J. and Shivpuri, R., 2004, "Prediction of chip morphology and segmentation during the machining of titanium alloys", *Journal of Materials Processing Technology*, Vol. 150, pp. 124-133.

Johnson, G.J. and Cook, W.H., 1983, "A constitutive model and data for metals subjected to large strains, high strain rates and high temperatures", Proceedings of the Seventh International Symposium on Ballistics, The Hague, pp.541-547.

Khan, A.S., Suh, Y.S. and Kazmi, R., 2004, "Quasi-static and dynamic loading responses and constitutive modeling of titanium alloys", *International Journal of Plasticity*, Vol. 20, pp. 2233-2248.

Lee, W.S. and Lin, C.F., 1998, "High temperature deformation behaviour of Ti6Al4V alloy evaluated by high strain rate compression tests", *Journal of Materials Processing Technology*, Vol. 75, pp. 127-136.

Lesuer, D.R., 2000, "Experimental investigations of material models for Ti–6Al–4V titanium and 2024-T3 aluminum". In: Final Report, DOT/FAA/AR-00/25, US Department of Transportation, Federal Aviation Administration**.**

Obikawa, T. and Usui, E., 1996, "Computational machining of titanium alloy – finite element modeling and a few results", *Transactions of the ASME*, Vol. 118, pp. 208-215.

Ozel, T. and Karpat, Y., 2007, "Identification of constitutive material model parameters for high strain rate metal cutting conditions using evolutionary computational algorithms", *Materials and Manufacturing Processes*, Vol. 22, pp. 659-667.

Shao, F., Liu, Z., Wan, Y. and Shi, Z., 2009, "Finite element simulation of machining of Ti-6Al-4V alloy with thermo dynamical constitutive equation", *International Journal of Advanced Manufacturing Technology*, Vol. 49, pp. 431-439.

Umbrello, D., 2008, "Finite element simulation of conventional and high speed machining of Ti6Al4V alloy", *Journal of Materials Processing Technology*, Vol. 196, pp. 79-87.

Vaz Jr, M., 2000, "On the numerical simulation of machining processes", *Journal of Brazilian Society of Mechanical Sciences*, Vol. 22, No. 2.